Soft dilepton production in relativistic heavy-ion collisions

K. Haglin,* C. Gale,† and V. Emel'yanov‡
Physics Deparment, McGill University, Montréal, P.Q., H3A 2T8, Canada
(Received 5 August 1992)

The production of electron-positron pairs with invariant masses less than 300 MeV from thermalized hadronic matter in relativistic heavy-ion collisions is calculated using a soft virtual photon approximation. The general theoretical framework is reviewed and extended to include arbitrarily massed and charged reaction partners, which we apply to pions and quarks. This result, exact within the soft photon approximation, is compared with a widely used approximate result which uses an electromagnetic amplitude limited in validity to momentum transfers less than $4m^2_{\pi(q)}$. This momentum-restricted method works very well for pions, constituent quarks and medium quarks, whereas it fails when applied to current quarks. A field-theory calculation is performed for the $\pi\pi$ elastic cross section which gives excellent agreement with data. Quark-antiquark annihilation diagrams in the Born approximation are estimated and compared with π^0 and η Dalitz decay contributions to the e^+e^- invariant-mass spectra. A comparison is made between the rate of production of zero total momentum soft dileptons obtained using resummation techniques in QCD perturbation theory and that which we calculate using this soft photon approximation. Then a Bjorken picture for the evolution is adopted allowing an integration over the history of the colliding nuclei. Using initial conditions likely to be found at the BNL Relativistic Heavy Ion Collider or CERN Large Hadron Collider we conclude even if Dalitz decays can be identified and subtracted from the experimental data it will be difficult to distinguish quark from pion degrees of freedom in the low-mass e^+e^- spectra.

PACS number(s): 12.38.Mh, 13.40.Ks, 25.75.+r

I. INTRODUCTION

Dileptons and photons [1–3] provide natural tools for observing thermalized nuclear matter. Once produced, they hardly interact and collide infrequently, if at all, with hadrons in a region of hot and dense matter. Therefore, photons and lepton pairs are among the best carriers of information about the earliest stages of the heavy-ion collision. In principle, they can carry information about the temperature of the primordial state. That there are many competing sources of photons and dileptons both before and after the hot stage of the collision makes reconstruction of the hottest state very difficult. The best that one can do is to evaluate the contribution from each source to ascertain whether or not it is dominant in some part of the phase space or if it has distinct properties rendering separation feasible. We proceed along these lines by considering four regions in the invariant mass M of the produced dileptons. For invariant masses M above the J/ψ peak, the spectrum is dominated by Drell-Yan production [2]. The spectrum around $M \simeq 1$ GeV is dominated by ρ, ω, and ϕ decays. Dileptons with invariant masses in the region 1.5–3.0 GeV seem to be mostly thermal [3]. Competing sources in this mass region are $D\bar{D}$ decays [4], and Drell-Yan and preequilibrium emission [5, 6]. Recent calculations [7] of dilepton spectra at invariant mass 1 GeV $< M <$ 3 GeV show that for presently achieved energy densities (CERN, BNL) the background is larger than thermal contributions. This is somewhat contrary to earlier calculations [8, 9], and the reason, in our opinion, is that the earlier calculations used initial temperatures and energy densities that were too high.

The last region of invariant mass ($M < m_\rho$), which we will consider in this paper, is a region of *soft* dilepton production [3]. There are many sources of dileptons with masses $M < m_\rho$: π^0 and η Dalitz decays, $\pi^+\pi^-$ annihilation (for $M^{e^+e^-} > 2m_\pi$), pion scattering with virtual bremsstrahlung, and if a quark-gluon plasma (QGP) is formed, there will be quark-antiquark annihilation and quark-quark(antiquark) scattering with virtual bremsstrahlung. Recent calculations [10, 11] have shown that in the mass region $M \simeq 2m_\pi$ the contribution from η Dalitz decay is two or thee orders of magnitude above $q\bar{q}$ annihilation spectra. But these calculations of the $q\bar{q}$ annihilation were done in the Born approximation. However, it has been shown [12] in the case of zero $p_\perp$ dileptons that for small mass pairs the perturbative corrections can be several order of magnitude larger than the Born term. The analysis has been extended to low invariant mass but large momenta with similar conclusions [13]. So we consider this $q\bar{q}$ annihilation spectra as a lower limit only.

The contribution of virtual bremsstrahlung from pion

*Electronic address: haglin@physics.mcgill.ca
†Electronic address: gale@physics.mcgill.ca
‡Permanent address: Department of High Energy Physics, Moscow Physical Engineering Institute, Kashirskoe Shosse 31, 115409, Moscow, Russia. Electronic address: vemel@hed.mephi.msk.su

scattering is the same order as η Dalitz decay in the mass region $M \simeq 2m_\pi$. This conclusion was reached by including only the processes $\pi^\pm\pi^0 \to \pi^\pm\pi^0\gamma^*$ [10]. There are other pion-pion reactions, such as $\pi^\pm\pi^\mp \to \pi^\pm\pi^\mp\gamma^*$, which will contribute to the overall e^+e^- spectrum. We will discuss such processes in this paper. Typically, a momentum transfer restriction ($|t| < 4m^2$) is the price to pay for a simple but approximate expression describing the electromagnetic factor in the cross section. Such expressions can be quite accurate when the masses are large, but for small massed particles such as current quarks, the approximation may not be so good. In this paper we relax this restriction on $|t|$ by considering scattering at any angles or energies for the charged particles. We will investigate the influence of such relaxation on the e^+e^- production rates and total yields.

If we consider $q\bar{q}$ annihilation in a QGP, it is also necessary to include quark (antiquark) and/or gluon scattering with virtual bremsstrahlung and their contribution to pair production. Their consideration is not possible without knowledge of the differential cross sections for quark-quark and quark-gluon elastic scattering. Using lattice gauge theory data on screening, we shall estimate the current ($m_q \simeq 5$ MeV), medium ($m_q = [2\pi\alpha_s/3]^{1/2}T$), and constituent ($m_q \simeq 300$ MeV) quark contributions to the electron-positron mass spectrum.

The paper is organized in the following way. In Sec. II we present the picture of evolution for the colliding nuclear system. In Sec. III we discuss the soft photon approximation for general *quasielastic* scattering with virtual bremsstrahlung and calculate the rate of e^+e^- production. The two contributing elements are the amplitude for elastic scattering and the polarization dotted into the electromagnetic current. We derive the exact electromagnetic factor and compare it with a popular approximate result, limited in validity to $|t| < 4m^2$. In Sec. IV we apply this formalism to thermalized pions at temperature T. Again, the exact and approximate results are presented. Then in Sec. V we use our formulas to calculate pair production through virtual bremsstrahlung in quark- (antiquark-)gluon and quark-quark (-antiquark) scattering. A comparison is made in Sec. VI among rates of zero (total) momentum pairs calculated using this soft photon approximation, QCD perturbation theory, and quark-antiquark annihilation with a modified dispersion relation. In order to obtain estimates for the total yields from these competing pion and quark processes, we integrate the rates over the time or temperature evolution of the colliding nuclei within a Bjorken picture [14] and present the results in Sec. VII. Also in Sec. VII we use isentropic evolution approximations to estimate π^0, η Dalitz decays and $q\bar{q}$ annihilation in the Born approximation. Finally, in Sec. VIII we write a brief summary and present concluding remarks.

II. EVOLUTION OF THE COLLIDING NUCLEAR SYSTEM

We assume formation of thermalized hadronic matter in relativistic heavy-ion collisions. This approach has recently been popularized especially with respect to QGP formation. There is evidence that in such collisions complete equilibration occurs within 1–2 fm/c [15]. The idea of thermalization is attractive because it enables us to use powerful methods from equilibrium thermodynamics. If the initial temperature $T_i > T_c \simeq 200$ MeV, then we expect hadrons to dissolve into freely propagating quarks, antiquarks, and gluons after having gone through a deconfinement phase transition. It is well known [3] that chiral invariance is restored near the phase transition temperature, whereupon constituent quarks ($m_q \simeq 300$ MeV) become current quarks with masses $m_q \simeq 5$ MeV. On the other hand, in a QGP the fermion mass induced by many-body effects is [3] $m_q = [2\pi\alpha_s(T)/3]^{1/2}T$. If we adopt the lattice gauge theory renormalization group result [16]

$$\alpha_s(T) = \frac{6\pi}{(33 - 2N_f)\ln(aT/T_c)}, \tag{2.1}$$

with $a \sim 8$, then for relevant temperatures $T \simeq 200$–300 MeV the medium quark masses $m_q \simeq 100$–150 MeV. So, if we want to calculate the bremsstrahlung contribution from the quark phase, it is necessary to take into account the processes of current and medium quark scattering at temperatures $T > T_c$ as well as constituent quark scattering at $T = T_c$. During a time evolution, the nuclear matter cools. If the QGP-hadron phase transition is first order at $T = T_c$, the mixed phase may be realized. In this case there is dilepton emission from current, medium, and constituent quarks, as well as from pion scattering with virtual bremsstrahlung. At $T = T_c$ nuclear matter transforms into an hadronic state, mainly of pions. For temperatures $T_c > T > T_f \simeq 140$ MeV, pion scattering with virtual quanta emission contributes. At the breakup temperature T_f we are left with only freely streaming particles.

III. SOFT VIRTUAL PHOTON APPROXIMATION

To begin the discussion, let us first recall some facts about bremsstrahlung in hadron-hadron collisions. If charged particles undergo acceleration, photons (real or virtual) may be radiated. Soft photon emission occurs

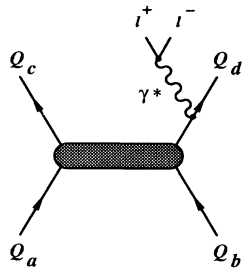

FIG. 1. Lepton pair production through virtual bremsstrahlung in scattering of particles $a\ b \to c\ d$. The particles might be charged or uncharged pions, quarks or antiquarks, or gluons. The shaded region indicates a strong interaction.

only from the external lines [17], as depicted in Fig 1. Relative to this, radiation from the strongly interacting blob is negligible. It continues to be negligible as long as the energy carried by the photon is less than the inverse of the strong interaction collision time $\tau \simeq 1$–2 fm/c, that is, if $E_\gamma \leq 100$–200 MeV. The advantage of the soft photon approximation is that the electromagnetic and strong interaction components of the matrix elements disentangle, leaving separate multiplicative factors. This allows the invariant cross section for scattering and at the same time producing a soft real photon of four-momentum q^μ to be written as [17]

$$q_0 \frac{d^4\sigma^\gamma}{d^3q\,dx} = \frac{\alpha}{4\pi^2}\left\{\sum_{\substack{\text{pol}\\ \lambda}} J\cdot\epsilon_\lambda\; J\cdot\epsilon_\lambda\right\}\frac{d\sigma}{dx}, \tag{3.1}$$

where $d\sigma/dx$ is the strong interaction cross section for the reaction $ab \to cd$, ϵ_λ is the polarization of the emitted photon, and

$$J^\mu = -Q_a\frac{p_a^\mu}{p_a\cdot q} - Q_b\frac{p_b^\mu}{p_b\cdot q} + Q_c\frac{p_c^\mu}{p_c\cdot q} + Q_d\frac{p_d^\mu}{p_d\cdot q}, \tag{3.2}$$

is the current. The Q's and p's represent the charges (in units of the proton charge) and the four-momenta of the particles, respectively. For soft virtual photons (dileptons) it is possible to continue from $q^2 = 0$ to $q^2 = M^2$, M being the invariant mass of the e^+e^- pair. The result is [17] ($q^\mu = p_+^\mu + p_-^\mu$)

$$E_+E_-\frac{d^6\sigma^{e^+e^-}}{d^3p_+d^3p_-} = \frac{\alpha}{2\pi^2}\frac{1}{q^2}q_0\frac{d^3\sigma^\gamma}{d^3q}. \tag{3.3}$$

Equations (3.1)–(3.3) can be combined to give the cross section for quasielastic $ab \to cd$ scattering while at the same time producing an e^+e^- pair. Four-momentum conservation is strictly enforced at the photon-dilepton vertices by writing

$$E_+E_-\frac{d\sigma^{e^+e^-}_{ab\to cd}}{d^3p_+d^3p_-} = \frac{\alpha^2}{8\pi^4}\frac{1}{M^2}\int |\epsilon\cdot J|^2_{ab\to cd}\frac{d\sigma_{ab\to cd}}{dt}\delta(q^2-M^2)dM^2\delta^4(q-(p_+ + p_-))d^4q\,dt, \tag{3.4}$$

where t is the four-momentum transfer in the $ab \to cd$ collision. The electromagnetic factor will be averaged over the photon's solid angle before insertion into Eq. (3.4). We note that this is somewhat different from the expression used by Gale and Kapusta [18], but this requires no further approximations, whereas in theirs q_0^2 was replaced with $(E_+ + E_-)[(E_+ + E_-)^2 - M^2]^{1/2}$ in order to facilitate analytic integration. Such a replacement introduces a slightly different mass dependence into the result than does Eq. (3.4). The ratio of Eq. (3.4) over the expression from Ref. [18] is equal to one in the limit of zero invariant mass and drops monotonically to zero in the limit of maximum invariant mass.

Separation of the full amplitude into strong and electromagnetic multiplicative factors is convenient. The strong interaction on-shell cross sections can be parametrized or modeled within, say, a quantum field theory. The electromagnetic factor can also be calculated exactly. It represents a coherent sum of all radiation fields involved, both initial and final charged states. Consider the completely general scattering process

$$ab \to cd, \tag{3.5}$$

where the masses $m_a = m_c$ and $m_b = m_d$ are arbitrary and the charges are subject only to overall charge conservation, namely, $Q_a + Q_b = Q_c + Q_d$. The exact squared modulus of the polarization dotted into the current for unequal masses is rather lengthy, and so it is presented in Appendix A. However, for equal-mass scattering it is

$$\begin{aligned}|\epsilon\cdot J|^2 = \frac{1}{q_0^2}\Bigg\{ &-(Q_a^2+Q_b^2+Q_c^2+Q_d^2) - 2(Q_aQ_b+Q_cQ_d)\frac{s-2m^2}{\sqrt{s(s-4m^2)}}\ln\left(\frac{\sqrt{s}+\sqrt{s-4m^2}}{\sqrt{s}-\sqrt{s-4m^2}}\right)\\ &+2(Q_aQ_d+Q_bQ_c)\frac{s-2m^2+t}{\sqrt{(s+t-4m^2)(s+t)}}\ln\left(\frac{\sqrt{s+t}+\sqrt{s+t-4m^2}}{\sqrt{s+t}-\sqrt{s+t-4m^2}}\right)\\ &+2(Q_aQ_c+Q_bQ_d)\frac{2m^2-t}{\sqrt{t(t-4m^2)}}\ln\left(\frac{\sqrt{4m^2-t}+\sqrt{-t}}{\sqrt{4m^2-t}-\sqrt{-t}}\right)\Bigg\},\end{aligned} \tag{3.6}$$

where $s \geq 4m^2$ and $-(s-4m^2) \leq t \leq 0$. This formula is very useful since it is valid for all energies and for all momentum transfers. It can be used to benchmark approximate expressions for $|\epsilon\cdot J|^2$, which is our next task. Suppose we have equal-mass scattering, charge conserved on each line, namely, $Q_a = Q_c$ and $Q_b = Q_d$, and finally, suppose the momentum transfer is small relative to the mass in the problem (specifically, $|t| < 4m^2$). Under these circumstances a good approximation to the electromagnetic factor is (for details see Appendix B)

$$|\epsilon\cdot J|^2_{ab\to cd} \simeq \frac{2}{3}\frac{1}{q_0^2}\left(\frac{-t}{m^2}\right)\left[(Q_a^2+Q_b^2) - \frac{3}{2}Q_aQ_bf(s)\right], \tag{3.7}$$

where

$$f(s) = \frac{s}{2(s-4m^2)} - \frac{s-4m^2}{2s} - \frac{m^2}{s}\left\{\frac{2\sqrt{s}}{\sqrt{s-4m^2}} + \left(\frac{\sqrt{s}}{\sqrt{s-4m^2}}\right)^3 + \frac{\sqrt{s-4m^2}}{\sqrt{s}}\right\}\ln\left(\frac{\sqrt{s}+\sqrt{s-4m^2}}{\sqrt{s}-\sqrt{s-4m^2}}\right). \tag{3.8}$$

The interference function is shown in Fig. 2. Its behavior is an amusing consequence of multipole interference. In the limit $\sqrt{s}/m \to 2$, $f(s) \to -2/3$, and as $\sqrt{s}/m \to \infty$, $f(s) \to 0$. Equations (3.7) and (3.8) are extremely useful because the result is linear in t. It turns out that this approximation is quite good as long as particles are at least as massive as pions. For processes involving lighter particles, one must resort to Eq. (3.6).

Whichever expression is used, either Eq. (3.6), Eq. (3.7), or the general form given in Appendix A, the common $1/q_0^2$ dependence allows analytic integration over the virtual photon and lepton momenta when inserted into Eq. (3.4). The resulting differential cross section is

$$\frac{d\sigma^{e^+e^-}_{ab\to cd}}{dM^2} = \frac{\alpha^2}{4\pi^2}\frac{\widehat{\sigma}(s)}{M^2}\left\{\ln\left(\frac{[\sqrt{s}-(m_a+m_b)]+\sqrt{[\sqrt{s}-(m_a+m_b)]^2-M^2}}{[\sqrt{s}-(m_a+m_b)]-\sqrt{[\sqrt{s}-(m_a+m_b)]^2-M^2}}\right) - \frac{2\sqrt{[\sqrt{s}-(m_a+m_b)]^2-M^2}}{[\sqrt{s}-(m_a+m_b)]}\right\}, \tag{3.9}$$

where we have defined

$$\widehat{\sigma}(s) \equiv \int_{-\lambda(s,m_a^2,m_b^2)/s}^{0} dt \frac{d\sigma_{ab\to cd}}{dt}\left(q_0^2|\epsilon\cdot J|^2_{ab\to cd}\right). \tag{3.10}$$

Sometimes known as the kinematic *triangle function*, $\lambda(x,y,z) = x^2 - 2(y+z)x + (y-z)^2$ [19]. Evaluation of the e^+e^- cross section proceeding along these lines neglects the momentum of the virtual photon in the phase-space δ function for the on-shell elastic cross section. Strictly speaking, one should correct for this by including the factor

$$\frac{R_2(s_2,m_a^2,m_b^2)}{R_2(s,m_a^2,m_b^2)} = \frac{\lambda^{1/2}(s_2,m_a^2,m_b^2)}{\lambda^{1/2}(s,m_a^2,m_b^2)}\frac{s}{s_2} \tag{3.11}$$

(with $s_2 = s + M^2 - 2\sqrt{s}q_0$) before integrating Eq. (3.4) [20]. We will include this correction in the numerical part of this study. The independent particle approximation from kinetic theory allows the rate (number of reactions per unit time per unit volume) to be written as

$$\frac{dN^{e^+e^-}_{ab}}{d^4x dM^2} = g_{ab}\int ds \int \frac{d^3p_a}{(2\pi)^3}\int \frac{d^3p_b}{(2\pi)^3} e^{-\beta(E_a+E_b)}\frac{d\sigma^{e^+e^-}_{ab}}{dM^2} v_{\rm rel}\delta(s-(p_a+p_b)^2), \tag{3.12}$$

where

$$v_{\rm rel} = \frac{\sqrt{(p_a\cdot p_b)^2 - m_a^2 m_b^2}}{E_a E_b},$$

β is the inverse temperature, and $g_{ab} = (2s_a+1)(2s_b+1)N_c^a N_c^b$ is the spin and color degeneracy. Integrating over both elastic scattering particles' momenta (for calculational details see Appendix C) yields

$$\frac{dN^{e^+e^-}_{ab}}{d^4x dM^2} = \frac{T^6 g_{ab}}{16\pi^4}\int_{z_{\rm min}}^{\infty} dz \frac{\lambda(z^2T^2,m_a^2,m_b^2)}{T^4} \times \mathcal{K}_1(z)\frac{d\sigma^{e^+e^-}_{ab}}{dM^2}(z), \tag{3.13}$$

where $z_{\rm min} = (m_a+m_b+M)/T$, $z = \sqrt{s}/T$, and $\mathcal{K}_1$ is a modified Bessel function. We are now in position to calculate the rate of electron-positron production through virtual bremsstrahlung from pion processes, quark-quark, or quark-gluon processes, etc.

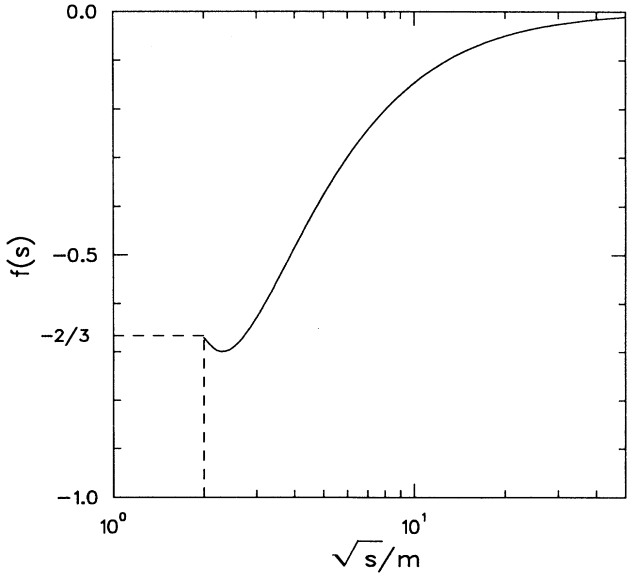

FIG. 2. Interference function $f(s)$ as it changes with the dimensionless variable $\sqrt{s}/m$.

IV. PAIR PRODUCTION FROM THERMALIZED PIONS

A truncated sum of the possible pion processes is used, that is,

$$\sum_{ab,cd} |\epsilon \cdot J|^2_{ab\to cd} \left(\frac{d\sigma}{dt}\right)_{ab\to cd} = |\epsilon \cdot J|^2_{\pi^+\pi^0} \left(\frac{d\sigma}{dt}\right)_{\pi^+\pi^0} + |\epsilon \cdot J|^2_{\pi^-\pi^0} \left(\frac{d\sigma}{dt}\right)_{\pi^-\pi^0} + |\epsilon \cdot J|^2_{\pi^+\pi^-} \left(\frac{d\sigma}{dt}\right)_{\pi^+\pi^-}. \tag{4.1}$$

We refer to this as truncated because with it we are neglecting $\pi^+\pi^+$ and $\pi^-\pi^-$ processes. Such an omission is justified by the fact their cross sections are smaller than the other isospin channels and there is significant cancellation due to destructive interference in like-charge processes [21]. We have also neglected $\pi^+\pi^- \to \pi^0\pi^0$, since $\sigma(\pi^+\pi^- \to \pi^0\pi^0)$ is rather small relative to the other pion processes [22]. Using the approximate electromagnetic amplitude, Eq. (3.4) becomes

$$\frac{d\sigma^{e^+e^-}_{\pi\pi}}{dM^2} = \frac{\alpha^2}{6\pi^2} \frac{\bar{\sigma}_{\pi\pi}(s)}{M^2} \Gamma(\sqrt{s}, m_\pi, M) \left\{\frac{4}{3} + \frac{1}{2} f(s)\right\}, \tag{4.2}$$

where $\sigma_{\pi\pi} \sim \sigma_{\pi^+\pi^0} + \sigma_{\pi^-\pi^0} + \sigma_{\pi^+\pi^-}$, the momentum transfer weighted cross section is $\bar{\sigma}(s)$, and we have defined yet another function

$$\Gamma(\sqrt{s}, m_\pi, M) = \ln\left(\frac{\sqrt{s} - 2m_\pi) + \sqrt{(\sqrt{s} - 2m_\pi)^2 - M^2}}{\sqrt{s} - 2m_\pi - \sqrt{(\sqrt{s} - 2m_\pi)^2 - M^2}}\right) - \frac{2\sqrt{(\sqrt{s} - 2m_\pi)^2 - M^2}}{\sqrt{s} - 2m_\pi}. \tag{4.3}$$

If $d\sigma/dt$ is a symmetric function of t and u, then [10]

$$\bar{\sigma}(s) = 2\sigma_{\rm el}(s)\left[\frac{s}{4m_\pi^2} - 1\right]. \tag{4.4}$$

The elastic pion-pion cross section is parametrized in the following way [10].

(a) For $\sqrt{s} \le 0.6$ GeV the chiral model expression is used:

$$\sigma_{\rm el}(s) = \frac{2}{3}\frac{1}{F_\pi^4}\frac{1}{16\pi} s\left[1 - \frac{5m_\pi^2}{s} + \frac{7m_\pi^4}{s^2}\right], \tag{4.5}$$

with the pion decay constant $F_\pi = 0.098$ GeV.

(b) At a collision energy near the ρ mass, $0.6 < \sqrt{s} \le 1.5$ GeV, the largest contribution to $\pi\pi$ the scattering amplitude is due to resonance formation. Therefore,

$$\sigma_{\rm el}(s) = \frac{g^4_{\rho\pi\pi}}{48\pi s} \frac{(s - 4m_\pi^2)^2}{(s - m_\rho^2)^2 + m_\rho^2\Gamma_\rho^2}, \tag{4.6}$$

where the coupling constant $g_{\rho\pi\pi} \simeq 6$, $m_\rho = 0.775$ GeV, and $\Gamma_\rho = 0.155$ GeV.

(c) For large collision energy $\sqrt{s} > 1.5$ GeV, $\sigma_{\rm el}$ becomes energy independent $\sigma_{\rm el} \simeq 5$ mb.

With a parametrization of the cross section we can combine Eqs. (3.13) and (4.2) to calculate the rate of e^+e^- production from the sum of $\pi^+\pi^0, \pi^-\pi^0$, and $\pi^+\pi^-$ processes. Different regions of $\sqrt{s}$ are investigated by varying the upper limit on the energy. The results at $T = 200$ MeV are presented in Fig. 3 along with a comparison of the rate using a quartic pion interaction $\mathcal{L}_I = \lambda(\boldsymbol{\pi} \cdot \boldsymbol{\pi})^2/4$ ($\lambda = 1.4$ from $\pi\pi$ scattering lengths) [23]. Our results reproduce the rate from the quartic interaction in the low-mass region $M < 100$ MeV only if $\sqrt{s}$ is restricted to the nonresonance region, say, $\sqrt{s} \le 0.45$ GeV. Electron-positron pairs with invariant masses larger than ~ 100 MeV are attributed to $\sqrt{s}$ in the resonance region and beyond.

Let us compare this production rate to a result which uses the exact electromagnetic factor. It is given by Eq. (3.6) with $Q_a, Q_b, Q_c, Q_d = 0, \pm 1$ and $m_a = m_b = m_\pi$. Since the t dependence is no longer linear, knowledge of the energy-dependent total elastic scattering cross section is not enough. We must have a parametrization or a model calculation of the differential cross section $d\sigma_{\rm el}/dt$ from which we integrate to obtain $\sigma_{\rm el}(s)$. We perform a field-theory calculation using σ, ρ, and $f(1270)$ meson

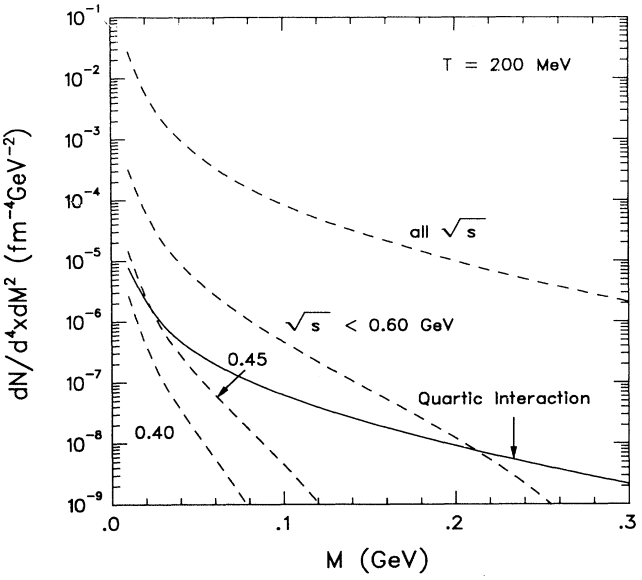

FIG. 3. (Approximate) e^+e^- production rates through virtual bremsstrahlung from pions as compared with quartic pion interaction predictions. The dashed lines are our estimations with varying values for the upper limit on the energy, and the solid line is from the quartic interaction.

exchange to model the strong interaction. The quantum numbers for these particles are $(I = 0, J = 0)$, $(I = 1, J = 1)$, and $(I = 0, J = 2)$, respectively. Low-energy $\pi\pi$ scattering length analyses suggest that momentum-dependent scalar and tensor couplings to the chiral fields should be used [24]. So the effective Lagrangian we use is

$$\mathcal{L}_{\rm int} = g_\sigma \sigma \partial_\mu \boldsymbol{\pi} \cdot \partial^\mu \boldsymbol{\pi} + g_\rho \boldsymbol{\rho}^{\,\mu} \cdot (\boldsymbol{\pi} \times \partial_\mu \boldsymbol{\pi}) + g_f f_{\mu\nu} \partial^\mu \boldsymbol{\pi} \cdot \partial^\nu \boldsymbol{\pi}. \tag{4.7}$$

Suppose we wish to calculate $\sigma(\pi^+\pi^- \to \pi^+\pi^-)$. The differential cross section is proportional to the square of the matrix element describing the overlap of initial and final two-hadron states. There are six terms in this matrix element: t- and s-channel σ-exchange, ρ-exchange, and f-exchange processes. The composite nature of the mesons necessitates modification at high momentum transfers. The net result is an effective suppression in that regime, and so the vertices in the t-channel diagrams are given momentum-transfer damping monopole form factors

$$h_\alpha(t) = \frac{m_\alpha^2 - m_\pi^2}{m_\alpha^2 - t}, \tag{4.8}$$

where m_α is either the σ, ρ, or the f mass depending upon which meson is exchanged.

In this model finite resonance lifetimes are incorporated into the scalar, vector, and tensor boson propagators. For the f propagator we use [25]

$$i\mathcal{P}^{\mu\nu\alpha\beta} = \frac{-i\left\{\frac{1}{2}\left(\frac{1}{3}g^{\mu\nu}g^{\alpha\beta} - g^{\mu\alpha}g^{\nu\beta} - g^{\mu\beta}g^{\nu\alpha}\right)\right\}}{k^2 - m_f^2 + i m_f \Gamma_f}. \tag{4.9}$$

As previously mentioned, there are six terms comprising the matrix element:

$$\mathcal{M} = \mathcal{M}_1 + \mathcal{M}_2 + \mathcal{M}_3 + \mathcal{M}_4 + \mathcal{M}_5 + \mathcal{M}_6, \tag{4.10}$$

where

$$\begin{aligned}
\mathcal{M}_1 &= \frac{-g_\sigma^2 h_\sigma^2(t)(2m_\pi^2 - t)^2}{t - m_\sigma^2 + i m_\sigma \Gamma_\sigma}, \\
\mathcal{M}_2 &= \frac{-g_\sigma^2 (s - 2m_\pi^2)^2}{s - m_\sigma^2 + i m_\sigma \Gamma_\sigma}, \\
\mathcal{M}_3 &= \frac{-g_\rho^2 h_\rho^2(t)(s - u)}{t - m_\rho^2 + i m_\rho \Gamma_\rho}, \\
\mathcal{M}_4 &= \frac{g_\rho^2 (u - t)}{s - m_\rho^2 + i m_\rho \Gamma_\rho}, \\
\mathcal{M}_5 &= \frac{g_f^2 h_f^2(t)}{t - m_f^2 + i m_f \Gamma_f} \\
&\quad \times \frac{1}{2}\left(\frac{1}{3}(2m_\pi^2 - t)^2 - (s - 2m_\pi^2)^2 - (2m_\pi^2 - u)^2\right), \\
\mathcal{M}_6 &= \frac{g_f^2}{s - m_f^2 + i m_f \Gamma_f} \\
&\quad \times \frac{1}{2}\left(\frac{1}{3}(s - 2m_\pi^2)^2 - (2m_\pi^2 - t)^2 - (2m_\pi^2 - u)^2\right).
\end{aligned} \tag{4.11}$$

Note that, as written, g_σ and g_f are not dimensionless, but $g_\sigma m_\sigma$ and $g_f m_f$ are. The full amplitude is symmetric under the interchange of the final states as required for bosons. The elastic differential cross section is

$$\frac{d\sigma}{dt} = \frac{|\mathcal{M}|^2}{16\pi s(s - 4m_\pi^2)}. \tag{4.12}$$

It has qualitatively the right behavior: For energies just below the ρ resonance the angular distribution is forwardly peaked, for $\sqrt{s}$ near m_ρ, the distribution becomes forward-backward symmetric, and finally above the resonance it is backward dominated. We can make a detailed comparison with data by integrating Eq. (4.12) in order to get $\sigma_{\rm el}(s)$. The scalar and tensor coupling constants and widths are adjusted so as to give resonant peaks which match experiment. Their numerical values along with the usual parameters for the ρ are $g_\sigma m_\sigma = 1.85$, $m_\sigma = 0.525$ GeV, $\Gamma_\sigma = 0.100$ GeV, $g_\rho = 6.15$, $m_\rho = 0.775$ GeV, $\Gamma_\rho = 0.155$ GeV, $g_f m_f = 7.2$, $m_f = 1.274$ GeV and $\Gamma_f = 0.176$ GeV. The results are shown in Fig. 4 along with experimental data from Refs. [26] and [27]. We obtain superb agreement with experiment for the energies shown. Other $\pi\pi$ processes $(\pi^\pm\pi^0 \to \pi^\pm\pi^0)$ proceed analogously. With all three cross sections, we can compute the rate of pair production using Eqs. (3.9) and (3.10), which is exact within the soft photon approximation. In Fig. 5 we show this rate along with the former (approximate) result of Eq. (4.2). The net result is a suppression from the approximate result by a mere factor ~ 2. Through this comparison we note that e^+e^- pairs with masses $\lesssim 100$ MeV are produced in $\pi\pi$ scattering at any kinematically allowed $\sqrt{s}$ and are therefore dominated near the ρ peak, whereas higher-mass pairs $(M \approx 300$ MeV) are effectively produced through $\pi\pi$ scattering with $\sqrt{s} \gtrsim m_\rho$. When $M \approx 300$ MeV in Eqs.

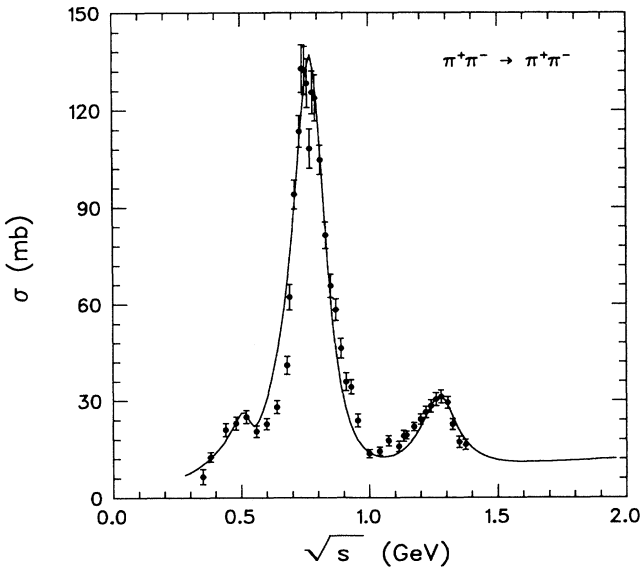

FIG. 4. Total elastic $\pi^+\pi^-$ cross section as compared with experimental data from Refs. [26] and [27].

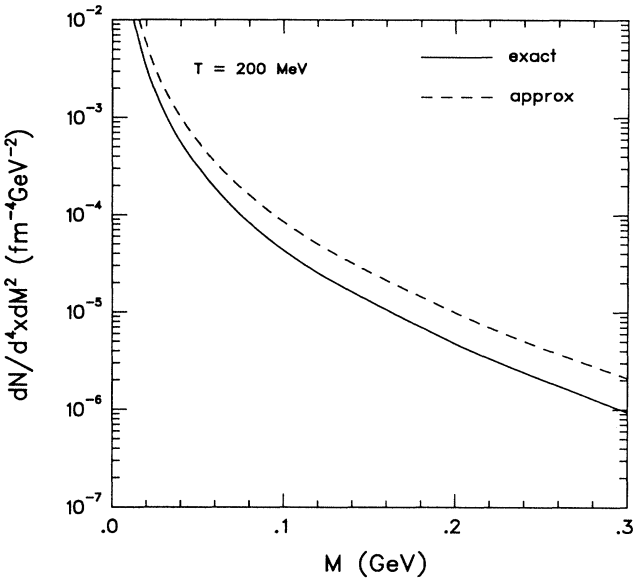

FIG. 5. e^+e^- production rates from pions using the exact electromagnetic factor and the model-calculated differential cross section (solid curve) as compared to the rate using the approximate electromagnetic expression and the assumed-symmetric parametrization of the total cross section (dashed curve).

(3.9) and (3.13) with $\sqrt{s}$ near the kinematically determined minimum (just below the ρ peak) the production rate is strongly suppressed by the logarithm and radical. Admittedly the soft photon approximation is less reliable for high masses, but this suggests that it is imperative to have a reasonably accurate calculation of the cross section for $\sqrt{s} > m_\rho$. Such a calculation would be incomplete if it excluded the tensor $f(1270)$ meson.

V. QUARK PROCESSES

Quark scattering processes introduce additional difficulties due to their fractional charge, their color, and their possibility for elastic scattering with their own force mediating bosons, the gluons. But we have developed the formalism to handle the general case. The same collection of diagrams from Fig. 1 is considered here with the charged external lines being u or d quarks (or antiquarks) and neutral external lines being gluons. In total we include six quark-quark (or antiquark) and four quark-gluon (or antiquark) diagrams. Other processes such as $q\bar{q} \to gg$ and its reverse process turn out to give a rather small contribution to the e^+e^- production rate (of order 8% of our chosen processes), and so we choose to neglect them here. It should also be mentioned that the approximate $|\epsilon \cdot J|^2$ cannot be applied to these. The electromagnetic amplitude for the quark-quark- (antiquark) processes is obtained from Eq. (3.6) by setting the mass to m_q and by setting Q_a and Q_b to the appropriate quark electric charges. For quark- (antiquark-)gluon process Eq. (A10) must be used with $m_a = m_q$ and $m_b = 0$. The strong interaction differential cross sections $d\sigma_{qq}/dt$ and $d\sigma_{qg}/dt$ are well known in the perturbative vacuum at the one-gluon-exchange level to be [28]

$$\frac{d\sigma_{ab}}{dt} = \frac{C_{ab} 2\pi\alpha_s^2}{t^2}, \tag{5.1}$$

where

$$C_{ab} = \begin{cases} 1 & (qg \to qg), \\ \frac{4}{9} & (qq \to qq). \end{cases} \tag{5.2}$$

For hot hadronic matter, this is clearly inadequate. Let us consider the dominant t-channel gluon-exchange amplitude for the diagram in Fig. 6: $\mathcal{M}^{ab} = \alpha_s \Gamma^a_\mu \mathcal{D}^{\mu\nu} \Gamma^b_\nu$, where $\mathcal{D}^{\mu\nu} = g^{\mu\nu}/t$ is the gluon propagator and $\Gamma^{a,b}_{\mu,\nu}$ are vertex functions for particles a,b. It is obvious that $\mathcal{M}^{ab}$ is singular in the zero-momentum-transfer limit. But at finite temperatures static color-electric fields are shielded by quarks and gluons in the plasma, and color-magnetic fields are also shielded by nonperturbative effects [29]. Color-electric shielding modifies the $\mu = \nu = 0$ components of $\mathcal{D}^{\mu\nu}$ in such a way that

$$\mathcal{M}^{ab}_E \simeq \alpha_s(t) \Gamma^a_0 \mathcal{D}^{00} \Gamma^b_0 \simeq \frac{\alpha_E(t)}{t} \Gamma^a_0 \Gamma^b_0, \tag{5.3}$$

where the running coupling constant [29]

$$\frac{\alpha_E(t)}{t} = \frac{\alpha_s(t)}{t - m_E^2} \tag{5.4}$$

and the color-electric mass $m_E^2 = 6\pi\alpha_s T^2$. For a medium-modified magnetic scattering amplitude we obtain

$$\mathcal{M}^{ab}_M \simeq \alpha_s(t) \Gamma^a_i \mathcal{D}^{ij} \Gamma^b_j \simeq -\frac{\alpha_M(t)}{t} \Gamma^a_i \Gamma^b_i, \tag{5.5}$$

where the effective magnetic coupling $\alpha_M(t)/t = \alpha_s(t)/(t - m_M^2)$ and the color-magnetic mass $m_M^2 = c\alpha_s^2 T^2$. Lattice gauge calculations [30] give $c \simeq 20$–30. In the small-t limit the vertex functions reduce to $\Gamma^a_\mu \simeq p^a_\mu$, where p^a_μ is the momentum of particle a. Averaging over color and spin degrees of freedom gives the differential cross section [29]

$$\frac{d\sigma_{ab}}{dt} = C_{ab} \frac{8\pi}{s^2 t^2} \left[\alpha_E(t) p^a_0 p^b_0 - \alpha_M(t) \mathbf{p}^a \cdot \mathbf{p}^b\right]^2, \tag{5.6}$$

where $s = (p_a + p_b)^2$.

Unfortunately, $d\sigma_{ab}/dt$ depends on the quark-quark (gluon) orientation in the scattering through $\mathbf{p}_a \cdot \mathbf{p}_b$. For

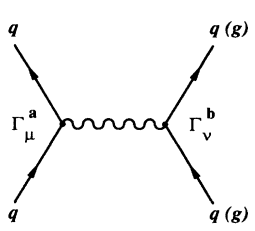

FIG. 6. t-channel gluon-exchange diagram.

arbitrary orientation of vectors $\mathbf{p}_a, \mathbf{p}_b$ we cannot obtain a closed expression for $d\sigma^{ab}/dt$, but if vector $\mathbf{p}_a$ is antiparallel to $\mathbf{p}_b$, $d\sigma_{ab}/dt$ reduces to

$$\frac{d\sigma^{ab}}{dt} = C_{ab}\frac{\pi}{2}\frac{\alpha_s^2(t)(2t - m_E^2 - m_M^2)^2}{(t - m_E^2)^2(t - m_M^2)^2}. \tag{5.7}$$

Note that this expression is exact for massless quark (antiquark) scattering. For $T \sim 200$–300 MeV, $\alpha_s \simeq 0.2$–0.3, $m_E \simeq 2.2T$, and $m_M \simeq 1.5T$. If we assume that the color-electric mass is roughly equal to the color-magnetic mass, $m_E \simeq m_M$, then we can restore the m_q dependence in the differential cross sections

$$\frac{d\sigma^{qg}}{dt} = \frac{2\pi\alpha_s^2(t)}{s^2(t - m_E^2)^2}(s - m_q^2)^2, \tag{5.8}$$

$$\frac{d\sigma^{qq}}{dt} = \frac{4}{9}\frac{2\pi\alpha_s^2(t)}{s^2(t - m_E^2)^2}(s - 2m_q^2)^2. \tag{5.9}$$

Using these expressions we did not observe sizable changes in the dilepton production rates or final spectra. So instead we use Eq. (5.7) henceforth. Note that in the limit $m_E, m_M \to 0$ (free space), we reproduce Eq. (5.1) for the perturbative vacuum.

Putting together Eqs. (3.4), (3.6), (3.13), and (5.7), we have the rate of e^+e^- production from all the quark-(antiquark-)gluon or quark- (antiquark-)quark processes. In Figs. 7 and 8 we compare usage of $|\epsilon \cdot J|^2_{\text{approx}}$ to usage of $|\epsilon \cdot J|^2_{\text{exact}}$ in calculating the rates of e^+e^- production from the sum of $qq(q\bar{q})$ and $qg(\bar{q}g)$ scattering with virtual bremsstrahlung at temperatures $T = 200$ and 300 MeV. Three quark curves are shown: current quarks, medium quarks, and constituent quarks with masses $m_q = 300$ MeV. A remarkable feature emerges in the comparison between the correct and approximate rates from current quarks: There is a huge suppression. To perhaps better understand this effect we present in Fig. 9 the ratio $R \equiv |\epsilon \cdot J|^2_{\text{exact}}/|\epsilon \cdot J|^2_{\text{approx}}$ for current, medium, and constituent u- and d-quark scattering at $\sqrt{s} = 775$ MeV.

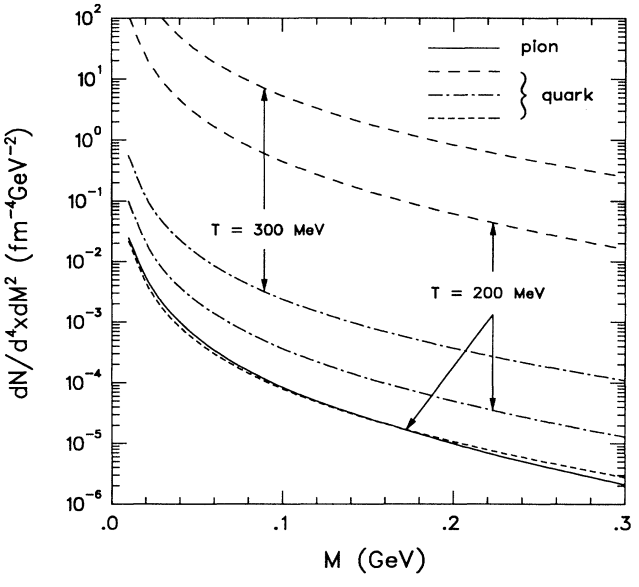

FIG. 7. Quark-driven rates at temperatures $T = 200$ and 300 MeV along with the pion-driven rate at T=200 MeV using the approximate electromagnetic factor applicable to each process. The long-dashed curves are for current quarks, the dot-dashed curves are medium quark results, and the short-dashed curve (also at $T = 200$ MeV) is for constituent quarks.

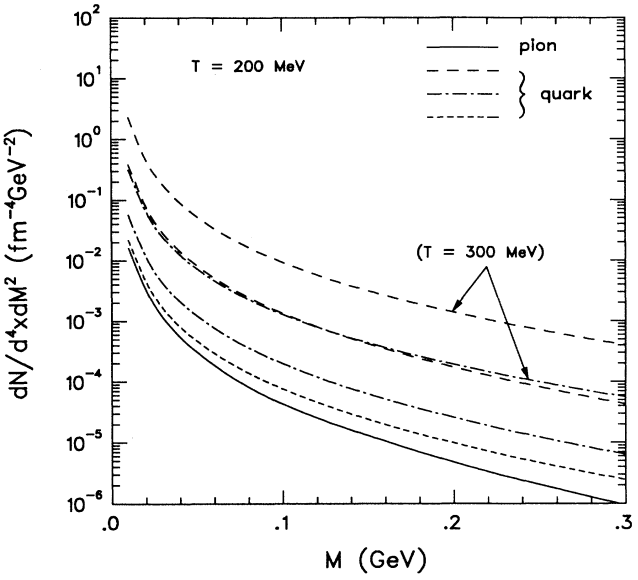

FIG. 8. Quark-driven rates superimposed on the pion-driven rate but this time using the correct electromagnetic factor. The labeling scheme is the same as the previous figure.

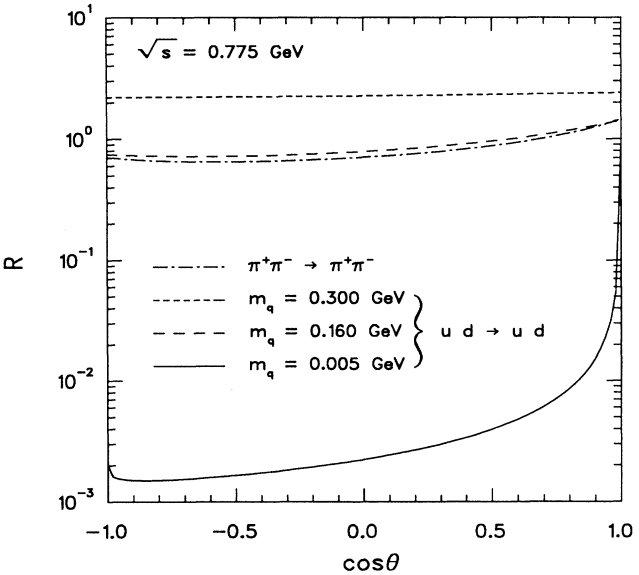

FIG. 9. Ratio $R \equiv |\epsilon \cdot J|^2_{\text{exact}}/|\epsilon \cdot J|^2_{\text{approx}}$ as it depends on the center-of-mass scattering angle $\cos\theta$.

Owing to the small mass of the current quarks, the resulting ratio is $R = 10^{-2}$–10^{-3}. Another interesting feature for current quarks is that $R \to 1$ as $\cos\theta \to 1$. Even at these (relativistic) energies, the electrodynamics in small-angle scattering is described very well by the approximate amplitude. However, these analyses invalidate Eq. (3.7) for high-momentum-transfer current quark scattering at these energies. Yet, for medium and constituent quarks, the ratio $R \sim 1$, and so for scattering of these particles the approximate expression [Eq. (3.7)] is rather good. Figure 9 also includes a curve for $\pi^+\pi^-$ scattering, where again the approximate electromagnetic factor is quite near the exact result.

Since the quark mass dependence in the production rate is roughly $1/m_q^2$ and the temperature dependence is roughly T^6, an upper limit on the rate is obtained using $m_q = 5$ MeV at $T = 300$ MeV. Similarly, a lower limit on the rate is obtained using $m_q = 300$ MeV at the phase transition temperature. Based on the results of Fig. 8 we conclude that at $T = 200$ MeV the (soft) virtual photon emissivities from competing medium quark versus pionic processes in the mass region $M \lesssim 2m_\pi$ differ by less than a factor 4. In a different energy regime Kapusta, Lichard, and Seibert [31] reached the same conclusion while comparing real (energetic) photon emissivities of the QGP to that of hadronic matter. This equal-luminous property appears also in the annihilation channels $q\bar{q} \to e^+e^-$ versus $\pi^+\pi^- \to \rho \to e^+e^-$ but only after an (invariant-mass) integrated total emissivity. In particular, the emissivities $dN^{e^+e^-}/d^4x$ at $T = 200$ MeV for pions, medium quarks, and constituent quarks are approximately $\simeq$2.5, 1.2, and $\simeq 1.1(\times 10^{-9}\ \mathrm{GeV}^4)$, respectively.

VI. ZERO- (TOTAL-) MOMENTUM PAIRS

As was pointed out by Kapusta [32], the production rate for soft dileptons could differ by orders of magnitude from the naive prediction of quark-antiquark annihilation. The enhancement might be due to a modification in the quark dispersion relation in thermalized hadronic matter. Furthermore, he argued that the zero-(total-) momentum e^+e^- mass spectrum is a direct measure of the quark dispersion relation and hence of chiral symmetry. A few possibilities for modifications are as follows. First, ignoring interactions with the matter would lead to a light-quark dispersion relation $\omega_1 = k$. Second, interactions with the plasma would result in a medium-quark dispersion relation $\omega_2 = (k^2+T^2)^{1/2}$. Still another possibility is to use weak-coupling methods self-consistently [33], where one possible parametrization is $\omega_3 = (\frac{1}{3} + k/T)k/(1 + k/T)$. Having a modified relation between energy and momentum for the quarks leads to a modification in the annihilation rates for producing zero-momentum lepton pairs. We can compare these rates with our soft photon approximation only at a qualitative level since one calculation includes scattering with bremsstrahlung and the other includes quark-antiquark annihilation. Nevertheless, it is interesting to see how they relate. Another result with which we might compare more quantitatively is one which uses the resummation techniques of Braaten and Pisarski [34]. They were recently applied [12] to a calculation of the zero-momentum soft dilepton production rate in a QGP. Here the differential rate for producing pairs is related to discontinuities in the photon self-energy. We refer the reader to Ref. [12] for further details and merely state the results. The partial rate from the annihilation and decay of soft quarks and antiquarks exhibits structure: sharp peaks due to Van Hove singularities. In addition to the pole contributions, there are terms resulting from cuts in the effective quark propagator. The square of a coherent sum of such contributions appears in the final answer. The physical processes which give the pole-cut and cut-cut contributions involve soft and hard quark-gluon scattering processes, which we have considered in our bremsstrahlung calculation. At small invariant mass, the pole-cut term grows like $\sim 1/M^2$ and the cut-cut term grows like $\sim 1/M^4$; they completely overwhelm the structure due to the pole-pole term.

In order to compare our result with either calculation mentioned, we must restrict the lepton pair to have zero total momentum $\mathbf{q} = 0$ in the rest frame of the matter. With such restrictions in Eq. (3.4), we cast the cross section into the form

$$\frac{d^4\sigma^{e^+e^-}}{dMd^3q}(\mathbf{q}=0) = \frac{\alpha^2}{4\pi^3}\frac{\widehat{\sigma}(s)}{M^4}, \tag{6.1}$$

where the weighted elastic cross section $\widehat{\sigma}(s)$ is that which we have defined in Eq. (3.10). The rate dN/d^4xdMd^3q ($\mathbf{q} = 0$) is then obtained by replacing $d\sigma/dM^2$ with $d^4\sigma/dMd^3q$ ($\mathbf{q} = 0$) in Eq. (3.12). In Fig. 10 we present the comparison of our (soft photon) approximate results for medium quarks, a parametrization of the results of Braaten, Pisarski, and Yuan [12] obtained using resummation techniques in QCD perturbation theory, along with the rate using the quark dispersion relation $\omega_3 = (1/3 + k/T)k/(1 + k/T)$ in the $q\bar{q}$ annihilation contribution. The other dispersion relations give even smaller rates. For dilepton masses $M \lesssim 0.1$ GeV, the production rate in the soft photon approximation is very near the result from QCD perturbation theory and much larger than the rate using the modified quark dispersion relation. Of course, the latter only includes annihilation, whereas the first two include scattering—so there is a qualitative difference. The low-mass dependence in the rates is $\sim 1/M^4$ both in the perturbation theory result as well as the soft photon approximation. This dependence is due to the processes of scattering hard quarks on hard gluons [12], which we have taken into account in the soft photon calculation. For masses $0.1 \lesssim M \lesssim 0.3$ GeV, the $\sim 1/M^2$ dependence starts to become significant in the perturbation theory result. As previously mentioned, this dependence is due to the pole-cut contributions or, physically, with scattering of soft quarks on hard gluons. These processes can only be included in our scheme by retaining the next-to-leading-order term in the soft photon approximation. The matrix element M^μ in a soft photon approximation is expanded in powers of the photon momentum q as

$$M^\mu = \frac{A^\mu}{q} + B^\mu + O(q), \tag{6.2}$$

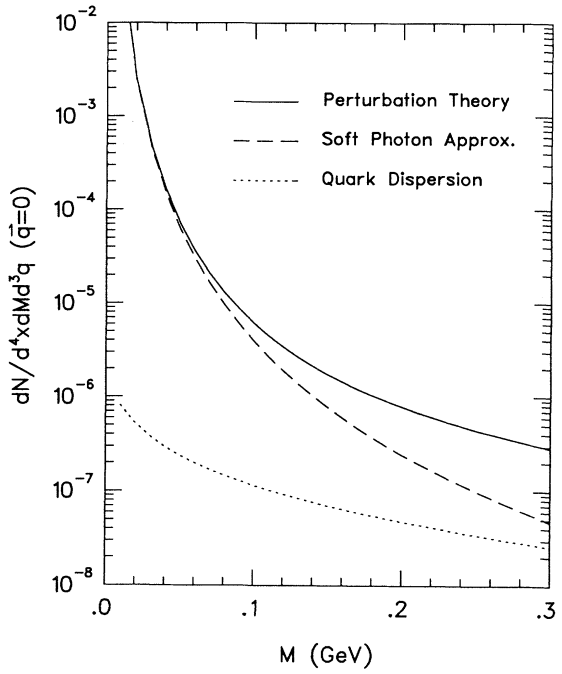

FIG. 10. Production rates for zero- (total-) momentum dileptons: The solid curve is a parametrization of the results from Ref. [12], the dashed curve is our soft photon approximate results, and the dotted curve is the result one gets by modifying the quark dispersion relation.

where both A^μ and B^μ may be calculated from knowledge of the physical, i.e., on-shell T matrix [35]. The term A^μ/q gives the $1/M^4$ dependence in dN/d^4xd^3q ($\mathbf{q} = 0$), while B^μ is responsible for next-to-leading-order terms. In particular, only $B^\mu \neq 0$ gives rise to $1/M^2$ dependence. The soft photon approximation with leading term only is quite close to the (resummed) perturbation theory result for masses $M \lesssim 0.1$ GeV. Most likely, the next-to-leading-order term (added coherently) would enhance the soft photon result for masses $0.1 \lesssim M \lesssim 0.3$ GeV by a factor of 2–6. However, such good agreement between our calculation and that of Ref. [12] does two things. It shows that scattering with virtual bremsstrahlung (rather than annihilation or Compton-like processes) accounts for most of the low-mass QGP-driven pairs, and second, it lends support to the validity of the soft-photon approximation as applied to quark processes.

VII. TOTAL ELECTRON-POSITRON YIELD

In the previous sections we calculated the rates of dilepton production by quark and pion scattering with virtual bremsstrahlung, i.e., the number of electron-positron pairs produced per unit four-volume d^4x and with mass M while being locally thermalized at temperature T. In order to obtain the spectrum with which to make an experimental comparison, it is necessary to integrate over the time evolution of the nuclear system. Such an integration is possible only after modeling the evolution in some way. We shall make the standard assumptions [14] about isentropic expansion and similarity flow in the central region ($y = 0$) of the heavy-ion collision. Under such assumptions the initial temperature and time can be related to the hadron distribution in the final phase (for $T_i > T_c$) by

$$T_i^3 \tau_i = \frac{c}{4a} \frac{1}{\pi R_A^2} \frac{dN^{AA\to\pi}}{dy}, \tag{7.1}$$

where $c \simeq 3.6$, $a \simeq 5.25$, R_A is the nuclear radius ($R_A = 7.1$ fm for Pb), and $\tau_i \simeq 1$ fm/c is the initial thermalization time. For energies reached at the BNL Relativistic Heavy Ion Collider (RHIC) and CERN Large Hadron Collider (LHC) the expected multiplicities $dN^{AA\to\pi}/dy \simeq 3000$ correspond to initial temperature $T_i \simeq 300$ MeV. As for the temperature of the phase transition T_c, the lattice estimations provide a range of $T_c \simeq$ 150–200 MeV. We assume that the phase transition is first order, and so at T_c the mixed phase may be realized. For possible decay temperatures we use $T_f = 140$ and 100 MeV. The production in the pure quark and hadronic phases can be calculated [9] from

$$\frac{dN^q}{dydM} = 3\pi R_A^2 T_i^6 \tau_i^2 \int_{T_c}^{T_i} \frac{dT}{T^7} \frac{dN^q}{d^4xdM} \tag{7.2}$$

and

$$\frac{dN^\pi}{dydM} = 3\pi R_A^2 T_i^6 \tau_i^2 r^2 \int_{T_f}^{T_c} \frac{dT}{T^7} \frac{dN^\pi}{d^4xdM}, \tag{7.3}$$

while the mixed phase contribution from quark and pion processes are

$$\frac{dN^q_{\text{mixed}}}{dydM} = \frac{\pi R_A^2}{2} \left(\frac{T_i}{T_c}\right)^6 \tau_i^2 (r-1) \frac{dN^q}{d^4xdM} \quad (T = T_c) \tag{7.4}$$

and

$$\frac{dN^\pi_{\text{mixed}}}{dydM} = \frac{\pi R_A^2}{2} \left(\frac{T_i}{T_c}\right)^6 \tau_i^2 r(r-1) \frac{dN^\pi}{d^4xdM} \quad (T = T_c). \tag{7.5}$$

Here r denotes the ratio of the number of degrees of freedom of the QGP constituents to that of the hadron gas constituents ($r \simeq 12$).

In Fig. 11 we present the resulting invariant-mass spectra through virtual bremsstrahlung from quarks and pions using relevant temperatures $T_i = 300$ MeV, $T_c = 200$ MeV, and $T_f = 140$ MeV. For this collection of temperatures the pion cooling phase contribution is the larger contributor to its final spectrum, whereas the mixed phase dominates the resulting quark-driven spectrum. Note the difference between the results here compared to our initial estimates in Fig. 4 of Ref. [11]. The suppression is due in part to the four-momentum conservation at the photon-dilepton vertices in Eq. (3.4) and to

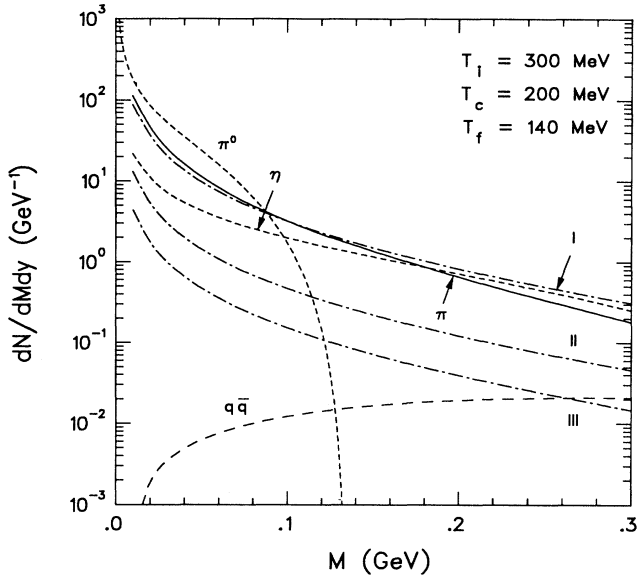

FIG. 11. Total e^+e^- yield from competing sources. The solid curve is for the pion-driven yield, the short-dashed curves are Dalitz decays, the long-dashed curve is the Born approximate $q\bar{q}$ annihilation result, and the dot-dashed curves are (I) current quarks, (II) medium quarks, and (III) constituent quarks.

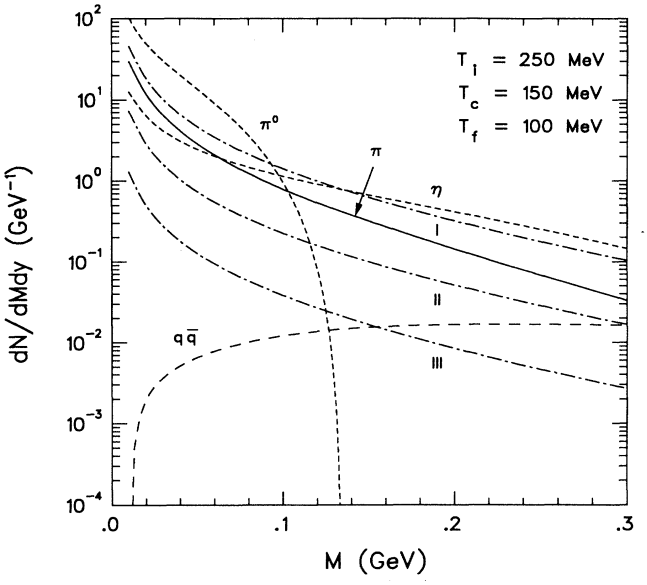

FIG. 12. Total e^+e^- yield with different relevant temperatures.

the phase-space correction shown in Eq. (3.11). Also included in Fig. 11 is an estimate of the background due to π^0 and η Dalitz decay $\pi^0 \to e^+e^- + \gamma$, $\eta \to e^+e^-\gamma$. We calculate these backgrounds using formulas from Ref. [10]. This comparison suggests that π^0 Dalitz decay is the strongest source of pairs having invariant mass less than the pion mass and that η Dalitz decay is the strongest source of e^+e^- pairs with invariant mass larger that m_π but less $2m_\pi$. For masses larger than $2m_\pi$, $\pi\pi$ annihilation will of course become dominant. Superimposed on Fig. 11 is also the yield from $q\bar{q} \to \gamma^* \to e^+e^-$ annihilation in the Born approximation [9, 10]. Throughout most of the range of dilepton invariant mass that we consider, the contributions from pion scattering with virtual bremsstrahlung and from π^0, η Dalitz decays are two or three orders of magnitude above the $q\bar{q}$ annihilation spectrum. Perturbative corrections to this annihilation spectrum for finite $p_\perp$ are extremely important [36]. An advantage of our soft photon approach is that we could easily evaluate the bremsstrahlung contribution at finite $q_\perp$ or even impose some cuts in transverse momentum.

Another quite reasonable possibility for the relevant temperatures of the colliding system is $T_i = 250$ MeV, $T_c = 150$ MeV, and $T_f = 100$ MeV, corresponding to those used in Ref. [10] in a recent study of low-mass dilepton production. We reproduce their $\pi^\pm\pi^0$ results using our $|\epsilon \cdot J|^2_{\text{approx}}$ and using the same parametrization of the total $\pi\pi$ cross section as did they. In Fig. 12 we show our *complete* calculation using these temperatures. Our final results are rather different from Ref. [10] since we include several improvements: We have other pion processes, we strictly conserve four-momentum at the photon-dilepton vertices, we use the exact electromagnetic factor, and finally, we correct phase space to include the momentum of the virtual photon. It should also be mentioned that the pion results of Ref. [10] should not be taken seriously for invariant masses larger than $\sim 2m_\pi$. They do not include any $\pi\pi$ resonances in the cross section with masses greater than the ρ, and most importantly they do not correct phase space, which is essential for higher invariant masses. For comparison purposes, we show in Fig. 13 still a different collection of

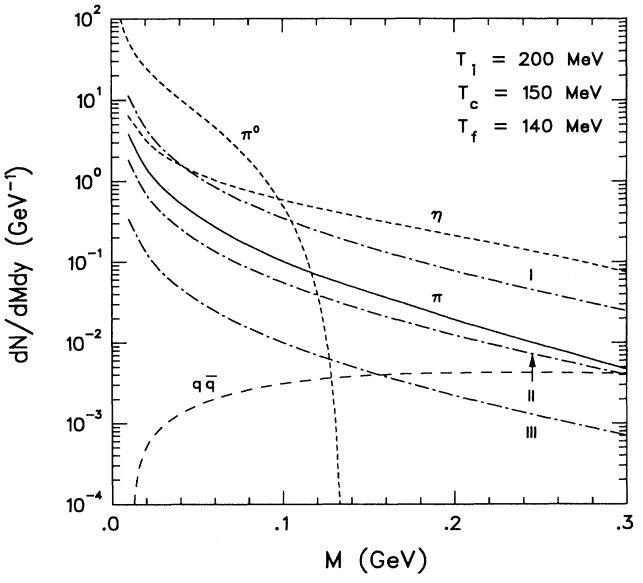

FIG. 13. Total e^+e^- yield with still a different set of relevant temperatures.

temperatures having the lowest T_c which is compatible with lattice gauge theory data—$T_i = 200$ MeV, $T_c = 150$ MeV, and $T_f = 140$ MeV. As one can see from Figs. 12 and 13, the medium-quark yield is always lower than the yields from π^0, η Dalitz decay as well as pion scattering with bremsstrahlung. This being true, detection of quark degrees of freedom within this invariant-mass region will be difficult in future heavy-ion experiments. Dalitz decays can (in principle) be distinguished from bremsstrahlung and removed from analyses. Distinguishing pairs produced through pion processes from those produced through *medium*-quark processes will be difficult since total yields from both are nearly the same in all temperature scenarios we investigated. However, these experiments may be very important with regard to the study of pion dynamics in a thermalized system. For initial temperatures $T_i > 350$ MeV ($dN/dy \gtrsim 4000$ for the LHC), pion bremsstrahlung is stronger than η Dalitz decay in the mass region $100 \lesssim M \lesssim 300$ MeV, but it is weaker than π^0 Dalitz decay for masses less than 100 MeV. From Eqs. (7.1)–(7.3), we see that the dilepton yield from thermalized pions is proportional to the square of the hadron multiplicity $(dN/dy)^2$, whereas it is directly proportional to the multiplicity for Dalitz decays. Therefore we expect that when the density of charged particles $dN/dy \gtrsim 4000$, the yield of e^+e^- pairs with $100 < M < 300$ MeV will be $\sim (dN/dy)^2$, but with $M \lesssim 100$ MeV it will be $\sim (dN/dy)$.

VIII. SUMMARY

In a relativistic heavy-ion collision there is likely born a hot thermalized system. We argued that one of the best probes of such a system must surely be electromagnetic in its nature. In this study we have used low-mass electron-positron pairs as such a vehicle by investigating their origin, abundance, and behavior during these collisions. A soft photon approximation was used to compare hadronic to partonic scattering with virtual bremsstrahlung. In particular, radiation of virtual quanta during $\pi\pi$ scattering with all isospin possibilities were discussed and compared with quark-quark-(antiquark) and quark- (antiquark-)gluon scattering accompanied by virtual radiation. We conclude that pions and medium quarks are roughly equally luminous at T_c, severely crippling our ability to separate one from the other.

We compared our quark-driven production rate for zero-momentum low-mass dileptons to that obtained using QCD resummation techniques. Our soft-photon-approximate result is very near the resummation rate for masses less than 100 MeV and a factor of 2–6 less than the resummation rate for masses larger than 100 (but less than 300 MeV). We expect that the next-to-leading-order term in the soft photon approximation (added coherently) would enhance our result for masses $0.1 \lesssim M \lesssim 0.3$ GeV by 2–6. Such good agreement for masses less than 100 MeV between our soft virtual photon calculation and that of Ref. [12] using resummation techniques lends support to the validity of the soft photon approach to this problem. Using a (1+1)-dimensional Bjorken hydrodynamic model to describe the expansion of the system, we calculated e^+e^- total yields for different collections of temperatures T_i, T_c, and T_f. For all reasonable sets of temperatures the constituent and the medium quark-driven total dilepton yields are lower than π^0 and η Dalitz decays and lower than the pion-driven yield. We must conclude that it will be difficult to observe quark degrees of freedom (DF) in this region of soft dileptons at LHC or RHIC. At the same time, it is important to keep in mind that our quark-driven soft-photon-approximate results were below the perturbation theory results (shown in Fig. 10) for invariant masses near $2m_\pi$ by a factor ~ 4. This precious factor of 4 may be enough to allow reasonably clear observation of these DF. Another useful observation is that for $T_i > 350$ MeV ($dN/dy \gtrsim 4000$ for LHC) the pion-driven production rate is larger than η Dalitz decay for masses $0.1 \lesssim M \lesssim 0.3$ GeV, though still smaller than π^0 Dalitz decay for masses smaller than 0.1 GeV. Therefore we predict that for $dN/dy \gtrsim 3000$ the yield of dileptons at $0.1 \lesssim M \lesssim 0.3$ GeV will be proportional to $(dN/dy)^2$, which reflects the collective effects in the thermalized pion gas; whereas the dilepton yield for $M \lesssim 0.1$ GeV is proportional to (dN/dy), i.e., π^0 Dalitz decay dominated. Future heavy-ion experiments (RHIC, LHC) will be useful for investigations of pion dynamics at high densities with regard to their soft dilepton mass spectra.

In our discussion of pion processes we assumed that the $\pi\pi$ differential cross section did not change from its free function at finite temperatures. In particular, we used the same expression for $d\sigma/dt$ and therefore $\sigma_{\rm el}$ near $T = T_c$ as we did for $T = 0$. It is clear that many-body effects introduce temperature dependences into the meson masses, widths, and coupling constants. Therefore the $\pi\pi$ elastic cross section will likely be quite different near T_c. In order to estimate the temperature dependence of $d\sigma_{\rm el}/dt$ and of $\sigma_{\rm el}$, we use as a first approximation the chiral perturbation theory modifications of F_π and Γ_ρ, which are [37]

$$F_\pi(T) = F_\pi(0)\left(1 - \frac{T^2}{8F_\pi^2(0)}\right) \tag{8.1}$$

and

$$\Gamma_\rho(T) = \frac{\Gamma_\rho(0)}{1 - T^2/4F_\pi^2(0)}. \tag{8.2}$$

The zero-temperature values are $F_\pi(0) \simeq 0.098$ GeV and $\Gamma_\rho(0) = 0.155$ GeV. Since the pion decay constant changes, so does the coupling of the ρ to the pions because $g_{\rho\pi\pi} = m_\rho/\sqrt{2}F_\pi$. The ρ-meson mass does not change appreciably with temperature [38]. We see from Eqs. (8.1) and (8.2) that the contribution of the nonresonance region ($\sqrt{s} \lesssim 0.6$ GeV) in $\sigma_{\rm el}$ will be enhanced with increasing T, whereas the contribution from the ρ resonace will be suppressed. Basically, the ρ-peak gets widened and reduced with increasing T. It gets completely melted at T_c. The spectrum $dN^{e^+e^-}/dMdy$ ob-

tained from Eq. (3.13) by some portion of a space-time integration for bremsstrahlung during pion scattering is proportional to the area under the $\sigma_{\rm el}(s)$ curve. Incorporating the temperature dependences in this fashion, we observe little or no change in this area. This translates into the fact that we do not observe a large difference (less than a factor 2 enhancement) in the production rates or total yield with a temperature-dependent cross section. Finally, we did not consider the change of $\Gamma_{\pi^0\to e^+e^-\gamma}$ or $\Gamma_{\eta\to e^+e^-\gamma}$ because the lifetime of the π^0 and the η is such that only very few will decay during the mixed or hadronic phases. So the pion bremsstrahlung contribution to the dilepton spectra is not very sensitive to temperature effects, if temperature dependences are well accounted by Eqs. (8.1) and (8.2).

One topic somewhat ignored in our study is the transverse momentum dependence of the produced e^+e^- pairs. Apart from the zero-momentum comparison we made, we presented all the results integrated over transverse momentum, mostly because this study represents a first detailed analysis of quark and pion bremsstrahlung. There are at least two reasons we might benefit from transverse momentum analyses. First, presentation of experimental data would most likely be $q_\perp$ restricted due to detector (in)efficiencies, and second there seems to be the possibility that Dalitz contributions might be suppressed more than would be bremsstrahlung for some restricted values of $q_\perp$ [39]. Finally, note that the soft photon approach that we have taken to this low-mass pair production problem can be equally well applied to the production of soft real photon production.

ACKNOWLEDGMENTS

One of us (V.E.) is grateful to Professor S. K. Mark and Professor P. Depommier for organizing his stay at McGill University and grateful to the Physics Department of McGill University for its warm hospitality. We acknowledge useful discussions with J. I. Kapusta, and P. Lichard. This work was supported in part by the Natural Sciences and Engineering Research Council of Canada, the FCAR fund of the Québec Government, and by a NATO collaborative research grant.

APPENDIX A: ELECTROMAGNETIC FACTOR $|\epsilon\cdot J|^2$

In this appendix we present the details for evaluating the exact electromagnetic factor for the soft photon approximation. Recall the current in the scattering process $ab\to cd$:

$$J^\mu=-Q_a\frac{p_a^\mu}{p_a\cdot q}-Q_b\frac{p_b^\mu}{p_b\cdot q}+Q_c\frac{p_c^\mu}{p_c\cdot q}+Q_d\frac{p_d^\mu}{p_d\cdot q}. \tag{A1}$$

Summing over polarizations aided by current conservation leads to [40]

$$\sum_{\rm pol}\epsilon_\mu\epsilon_\nu J^\mu J^\nu=-J^2. \tag{A2}$$

The particles' initial velocities are β_a,β_b and final velocities are β_c,β_d ($c=1$). Since $p_i^2=m_i^2$, we have

$$\begin{aligned}|\epsilon\cdot J|^2=&-\frac{Q_a^2m_a^2}{E_a^2q_0^2(1-\beta_a\cdot\mathbf{n})^2}-\frac{Q_b^2m_b^2}{E_b^2q_0^2(1-\beta_b\cdot\mathbf{n})^2}-\frac{Q_c^2m_c^2}{E_c^2q_0^2(1-\beta_c\cdot\mathbf{n})^2}\\&-\frac{Q_d^2m_d^2}{E_d^2q_0^2(1-\beta_d\cdot\mathbf{n})^2}-\frac{2Q_aQ_b(1-\beta_a\cdot\beta_b)}{q_0^2(1-\beta_a\cdot\mathbf{n})(1-\beta_b\cdot\mathbf{n})}+\frac{2Q_aQ_c(1-\beta_a\cdot\beta_c)}{q_0^2(1-\beta_a\cdot\mathbf{n})(1-\beta_c\cdot\mathbf{n})}\\&+\frac{2Q_aQ_d(1-\beta_a\cdot\beta_d)}{q_0^2(1-\beta_a\cdot\mathbf{n})(1-\beta_d\cdot\mathbf{n})}+\frac{2Q_bQ_c(1-\beta_b\cdot\beta_c)}{q_0^2(1-\beta_b\cdot\mathbf{n})(1-\beta_c\cdot\mathbf{n})}\\&+\frac{2Q_bQ_d(1-\beta_b\cdot\beta_d)}{q_0^2(1-\beta_b\cdot\mathbf{n})(1-\beta_d\cdot\mathbf{n})}-\frac{2Q_cQ_d(1-\beta_c\cdot\beta_d)}{q_0^2(1-\beta_c\cdot\mathbf{n})(1-\beta_d\cdot\mathbf{n})},\end{aligned} \tag{A3}$$

where $\mathbf{n}\equiv\mathbf{q}/|\mathbf{q}|$ is the unit vector for the photon. We are interested in an angular average over the emitted photon's direction

$$\int\frac{d\Omega_q}{4\pi}|\epsilon\cdot J|^2. \tag{A4}$$

Carrying out the integrals for the first four terms in Eq. (A3) is elementary. The result for each is just the charge squared over q_0^2. The remaining terms (identical in structure) are readily evaluated using a two-parameter Feynman integral

$$\frac{1}{ab}=\int_0^1\frac{dx}{[ax+b(1-x)]^2}. \tag{A5}$$

We show the technique for evaluating the general case and then apply it to the remaining terms in Eq. (A3). The integral under question is

$$\begin{aligned}\mathcal{I}(\mathbf{u},\mathbf{v}) &= \int \frac{d\Omega_n}{4\pi}\frac{1}{(1-\mathbf{u}\cdot\mathbf{n})(1-\mathbf{v}\cdot\mathbf{n})} \\ &= \int_0^1 dx \int \frac{d\Omega_n}{4\pi}\frac{1}{\{1-\mathbf{n}\cdot[\mathbf{u}x+\mathbf{v}(1-x)]\}^2} \\ &= \int_0^1 dx \frac{1}{\left(1-|\mathbf{u}x+\mathbf{v}(1-x)|^2\right)} \\ &= \frac{1}{-|\mathbf{u}-\mathbf{v}|^2}\int_0^1 dx \frac{1}{\left(x+\frac{v^2-\mathbf{u}\cdot\mathbf{v}}{-|\mathbf{u}-\mathbf{v}|^2}\right)^2 - \left(\frac{\sqrt{(1-\mathbf{u}\cdot\mathbf{v})^2-(1-u^2)(1-v^2)}}{-|\mathbf{u}-\mathbf{v}|^2}\right)^2}. \end{aligned} \tag{A6}$$

Decompose the integrand into fractions whose denominators are linear in x at which point integration is trivial. We obtain the closed form expression

$$\mathcal{I}(\mathbf{u},\mathbf{v}) = \frac{1}{2\sqrt{\mathcal{D}_{uv}}}\ln\left|\frac{[\mathbf{u}\cdot\mathbf{v}-u^2-\sqrt{\mathcal{D}_{uv}}\,][\mathbf{u}\cdot\mathbf{v}-v^2-\sqrt{\mathcal{D}_{uv}}\,]}{[\mathbf{u}\cdot\mathbf{v}-u^2+\sqrt{\mathcal{D}_{uv}}\,][\mathbf{u}\cdot\mathbf{v}-v^2+\sqrt{\mathcal{D}_{uv}}\,]}\right|, \tag{A7}$$

where

$$\mathcal{D}_{uv} = (1-\mathbf{u}\cdot\mathbf{v})^2-(1-u^2)(1-v^2). \tag{A8}$$

The net result of applying this to the relevant terms in Eq. (A3) is

$$\begin{aligned}|\epsilon\cdot J|^2 = \frac{1}{q_0^2}\ \{&-(Q_a^2+Q_b^2+Q_c^2+Q_d^2) - 2Q_aQ_b(1-\boldsymbol{\beta}_a\cdot\boldsymbol{\beta}_b)\mathcal{I}(\boldsymbol{\beta}_a,\boldsymbol{\beta}_b) \\ &-2Q_cQ_d(1-\boldsymbol{\beta}_c\cdot\boldsymbol{\beta}_d)\mathcal{I}(\boldsymbol{\beta}_c,\boldsymbol{\beta}_d) + 2Q_aQ_c(1-\boldsymbol{\beta}_a\cdot\boldsymbol{\beta}_c)\mathcal{I}(\boldsymbol{\beta}_a,\boldsymbol{\beta}_c) \\ &+2Q_bQ_d(1-\boldsymbol{\beta}_b\cdot\boldsymbol{\beta}_d)\mathcal{I}(\boldsymbol{\beta}_b,\boldsymbol{\beta}_d) + 2Q_aQ_d(1-\boldsymbol{\beta}_a\cdot\boldsymbol{\beta}_d)\mathcal{I}(\boldsymbol{\beta}_a,\boldsymbol{\beta}_d) + 2Q_bQ_c(1-\boldsymbol{\beta}_b\cdot\boldsymbol{\beta}_c)\mathcal{I}(\boldsymbol{\beta}_b,\boldsymbol{\beta}_c)\}. \end{aligned} \tag{A9}$$

In order to write this in terms of invariants it is perhaps easiest to move to the center-of-momentum (c.m.) frame and write

$$\begin{aligned}|\epsilon\cdot J|^2_{ab\to cd} = \frac{1}{q_0^2}\ \{&-(Q_a^2+Q_b^2+Q_c^2+Q_d^2) - 2(Q_aQ_b+Q_cQ_d)\mathcal{F}(\boldsymbol{\beta}_a^*,\boldsymbol{\beta}_b^*) \\ &+2(Q_aQ_c+Q_bQ_d)\mathcal{F}(\boldsymbol{\beta}_a^*,\boldsymbol{\beta}_c^*) + 2(Q_aQ_d+Q_bQ_c)\mathcal{F}(\boldsymbol{\beta}_a^*,\boldsymbol{\beta}_d^*)\}, \end{aligned} \tag{A10}$$

where the function

$$\begin{aligned}\mathcal{F}(\mathbf{x},\mathbf{y}) = \frac{(1-\mathbf{x}\cdot\mathbf{y})}{2\sqrt{(1-\mathbf{x}\cdot\mathbf{y})^2-(1-x^2)(1-y^2)}}\Bigg\{ &\ln\left|\frac{\mathbf{x}\cdot\mathbf{y}-x^2-\sqrt{(1-\mathbf{x}\cdot\mathbf{y})^2-(1-x^2)(1-y^2)}}{\mathbf{x}\cdot\mathbf{y}-x^2+\sqrt{(1-\mathbf{x}\cdot\mathbf{y})^2-(1-x^2)(1-y^2)}}\right| \\ &+\ln\left|\frac{\mathbf{x}\cdot\mathbf{y}-y^2-\sqrt{(1-\mathbf{x}\cdot\mathbf{y})^2-(1-x^2)(1-y^2)}}{\mathbf{x}\cdot\mathbf{y}-y^2+\sqrt{(1-\mathbf{x}\cdot\mathbf{y})^2-(1-x^2)(1-y^2)}}\right|\Bigg\} \end{aligned} \tag{A11}$$

and the c.m. velocities can be related to (Mandelstam) invariants through

$$\begin{aligned}\boldsymbol{\beta}_a^*\cdot\boldsymbol{\beta}_b^* &= \frac{-\lambda(s,m_a^2,m_b^2)}{(s+m_a^2-m_b^2)(s-m_a^2+m_b^2)}, \\ \boldsymbol{\beta}_a^*\cdot\boldsymbol{\beta}_c^* &= \frac{\lambda(s,m_a^2,m_b^2)}{(s+m_a^2-m_b^2)^2}\left(1+\frac{2st}{\lambda(s,m_a^2,m_b^2)}\right), \\ \boldsymbol{\beta}_a^*\cdot\boldsymbol{\beta}_d^* &= \frac{-\lambda(s,m_a^2,m_b^2)}{(s+m_a^2-m_b^2)(s-m_a^2+m_b^2)} \\ &\quad\times\left(1+\frac{2st}{\lambda(s,m_a^2,m_b^2)}\right) \end{aligned} \tag{A12}$$

and

$$\begin{aligned}(\beta_a^*)^2 = (\beta_c^*)^2 &= \frac{\lambda(s,m_a^2,m_b^2)}{(s+m_a^2-m_b^2)^2}, \\ (\beta_b^*)^2 = (\beta_d^*)^2 &= \frac{\lambda(s,m_a^2,m_b^2)}{(s-m_a^2+m_b^2)^2}. \end{aligned} \tag{A13}$$

APPENDIX B: APPROXIMATE ELECTROMAGNETIC FACTOR

It is perhaps more convenient to have an approximate, yet reasonably reliable expression for $|\epsilon\cdot J|^2$. This appendix is devoted to such a calculation. We must restrict

our attention in this section to equal-mass scattering. Let $p_a^\mu = (E_a, \mathbf{p}_a)$ be the four-vector for particle a, and similarly for particles b, c, and d. Let $q^\mu = q_0(1, \mathbf{n})$ again be the photon's spacetime description and choose the radiation gauge so that $\epsilon^\mu = (0, \boldsymbol{\epsilon})$. Then the quantity $|\epsilon \cdot J|^2$ can be written

$$|\epsilon \cdot J|^2 = \frac{1}{q_0^2}\left|\boldsymbol{\epsilon} \cdot \left(\frac{Q_c \boldsymbol{\beta}_c}{1 - \mathbf{n}\cdot\boldsymbol{\beta}_c} - \frac{Q_a \boldsymbol{\beta}_a}{1 - \mathbf{n}\cdot\boldsymbol{\beta}_a} + \frac{Q_d \boldsymbol{\beta}_d}{1 - \mathbf{n}\cdot\boldsymbol{\beta}_d} - \frac{Q_b \boldsymbol{\beta}_b}{1 - \mathbf{n}\cdot\boldsymbol{\beta}_b}\right)\right|^2 . \quad \text{(B1)}$$

Let us work in the c.m. frame, which allows us to write $\boldsymbol{\beta}_a = \boldsymbol{\beta}$, $\boldsymbol{\beta}_c = \boldsymbol{\beta} + \Delta\boldsymbol{\beta}$, $\boldsymbol{\beta}_b = -\boldsymbol{\beta}$, and $\boldsymbol{\beta}_d = -(\boldsymbol{\beta} + \Delta\boldsymbol{\beta})$. We also assume that $Q_a = Q_c$, $Q_b = Q_d$. Then, if the scattering is such that $\Delta\boldsymbol{\beta}$ is small relative to $\boldsymbol{\beta}$, a good approximation to Eq. (B1) is

$$\simeq \frac{1}{q_0^2}\left|\boldsymbol{\epsilon} \cdot \left(\frac{Q_a[\Delta\boldsymbol{\beta} + \mathbf{n} \times (\boldsymbol{\beta} \times \Delta\boldsymbol{\beta})]}{(1 - \mathbf{n}\cdot\boldsymbol{\beta})^2} + \frac{Q_b\,(-\Delta\boldsymbol{\beta} + \mathbf{n} \times (\boldsymbol{\beta} \times \Delta\boldsymbol{\beta})}{(1 + \mathbf{n}\cdot\boldsymbol{\beta})^2}\right)\right|^2 , \quad \text{(B2)}$$

where $\boldsymbol{\beta}$ is the initial (or average) velocity. Since we consider small-angle deflection, $\Delta\boldsymbol{\beta}$ is approximately perpendicular to the incident direction. Next we explicitly sum over polarizations by defining the unit vectors $\hat{\epsilon}_\parallel$ and $\hat{\epsilon}_\perp$ to be the polarization vectors parallel and perpendicular to the plane containing $\boldsymbol{\beta}$ and $\mathbf{n}$. Averaging over the azimuth of the scattered particles, the two polarization summands become

$$|\epsilon \cdot J|_\parallel^2 = \frac{|\Delta\boldsymbol{\beta}|^2}{2q_0^2}\int \frac{d\Omega}{4\pi}\left(\frac{Q_a}{1 - \beta\cos\theta} + \frac{Q_b}{1 + \beta\cos\theta}\right)^2 \quad \text{(B3)}$$

and

$$|\epsilon \cdot J|_\perp^2 = \frac{|\Delta\boldsymbol{\beta}|^2}{2q_0^2}\int \frac{d\Omega}{4\pi}\left(\frac{Q_a(\beta - \cos\theta)}{(1 - \beta\cos\theta)^2} + \frac{Q_b(\beta + \cos\theta)}{(1 + \beta\cos\theta)^2}\right)^2 . \quad \text{(B4)}$$

Integration of these expressions is elementary but quite lengthy. We perform the necessary work and add the contributions from both polarizations to get

$$|\epsilon \cdot J|^2_{\text{approx}} = \frac{|\Delta\boldsymbol{\beta}|^2\gamma^2}{q_0^2}\left\{\frac{Q_a^2}{6} + \frac{Q_b^2}{6} + \frac{Q_a^2 + Q_b^2}{2} + \beta\frac{Q_a Q_b}{2} - \frac{1}{\beta^2}\frac{Q_a Q_b}{2} + \frac{Q_a Q_b}{2\gamma^2}\left[\frac{1}{\beta} + \frac{1}{2\beta^3} + \frac{\beta}{2}\right]\ln\left(\frac{1+\beta}{1-\beta}\right)\right\}. \quad \text{(B5)}$$

The change in velocity is, of course, related to the momentum transfer through $\gamma^2|\Delta\boldsymbol{\beta}|^2 = -t/m^2$ and the velocity is related to the total energy through $\beta^2 = (s - 4m^2)/s$. Restoring the invariants s and t, we get the final (approximate) result of

$$|\epsilon \cdot J|^2_{\text{approx}} = \frac{2}{3}\frac{1}{q_0^2}\left(\frac{-t}{m^2}\right)\left[(Q_a^2 + Q_b^2) - \frac{3}{2}Q_a Q_b f(s)\right], \quad \text{(B6)}$$

where

$$f(s) = \frac{s}{2(s - 4m^2)} - \frac{s - 4m^2}{2s} - \frac{m^2}{s}\left\{\frac{2\sqrt{s}}{\sqrt{s - 4m^2}} + \left(\frac{\sqrt{s}}{\sqrt{s - 4m^2}}\right)^3 + \frac{\sqrt{s - 4m^2}}{\sqrt{s}}\right\}\ln\left(\frac{\sqrt{s} + \sqrt{s - 4m^2}}{\sqrt{s} - \sqrt{s - 4m^2}}\right). \quad \text{(B7)}$$

Strictly speaking, this expression is valid only for $|t| < 4m^2$.

APPENDIX C: RATE CALCULATION FROM GENERAL SCATTERING PROCESS

The starting point for the rate calculation (from kinetic theory) is

$$\frac{dN_{ab}^{e^+e^-}}{d^4x dM^2} = g_{ab}\int ds \int \frac{d^3p_a}{(2\pi)^3}\int \frac{d^3p_b}{(2\pi)^3}e^{-\beta(E_a+E_b)}\frac{d\sigma(s)}{dM^2} \times v_{\text{rel}}\delta(s - (p_a + p_b)^2), \quad \text{(C1)}$$

where $g_{ab} = (2s_a + 1)(2s_b + 1)N_c^a N_c^b$ is the (spin and color) degeneracy. Trivial angular integrations can be done,

$$\frac{dN_{ab}^{e^+e^-}}{d^4x dM^2} = \frac{g_{ab}}{32\pi^4}\int ds \int dp_a \int dp_b \frac{p_a p_b e^{-\beta(E_a+E_b)}}{E_a E_b} \times \frac{d\sigma_{ab}^{e^+e^-}}{dM^2}\lambda^{1/2} \times (s, m_a^2, m_b^2)\Theta(\chi) \quad \text{(C2)}$$

where

$$\lambda(s, m_a^2, m_b^2) = s\,(s - 2[m_a^2 + m_b^2]) + (m_a^2 - m_b^2)^2 \quad \text{(C3)}$$

and

$$\chi = [4E_aE_b(s - m_a^2 - m_b^2) - (s - m_a^2 - m_b^2)^2 - 4m_a^2E_b^2 - 4m_b^2E_a^2 + 4m_a^2m_b^2]. \quad \text{(C4)}$$

Using the substitutions

$$u = E_a + E_b \qquad \text{and} \qquad v = E_a - E_b, \quad \text{(C5)}$$

the differential element changes, due to the fact that the Jacobian is different from 1, as follows

$$dE_a dE_b \rightarrow \frac{dudv}{2}. \quad \text{(C6)}$$

Completing the substitution, we get

$$\frac{dN_{ab}^{e^+e^-}}{d^4xdM^2} = \frac{g_{ab}}{64\pi^4}\int ds \int dv \int_{u_-}^{u_+} du\, e^{-\beta v}\frac{d\sigma_{ab}^{e^+e^-}}{dM^2} \times \lambda^{1/2}(s, m_a^2, m_b^2), \quad \text{(C7)}$$

where

$$u_\pm = \frac{v(m_a^2 - m_b^2)}{s} \pm \left(\frac{\lambda^{1/2}(s, m_a^2, m_b^2)}{s}\right)\sqrt{v^2 - s}. \quad \text{(C8)}$$

After integrating over u, the remaining v integration can only be written in terms of a modified Bessel function. The rate is

$$\frac{dN_{ab}^{e^+e^-}}{d^4xdM^2} = \frac{g_{ab}}{32\pi^4}\int ds\, \lambda(s, m_a^2, m_b^2)\frac{\mathcal{K}_1(\beta\sqrt{s})}{\beta\sqrt{s}}\frac{d\sigma_{ab}^{e^+e^-}}{dM^2}. \quad \text{(C9)}$$

Introducing the dimensionless variable $z = \sqrt{s}/T$, we arrive at the final expression

$$\frac{dN_{ab}^{e^+e^-}}{d^4xdM^2} = \frac{T^6 g_{ab}}{16\pi^4}\int_{z_{\min}}^{\infty} dz \frac{\lambda(z^2T^2, m_a^2, m_b^2)}{T^4} \times \mathcal{K}_1(z)\frac{d\sigma_{ab}^{e^+e^-}}{dM^2}(z), \quad \text{(C10)}$$

where $z_{\min} = (m_a + m_b + M)/T$.

[1] E. Feinberg, Nuovo Cimento A **34**, 39 (1976).
[2] E. Shuryak, Phys. Lett. **79B**, 135 (1978).
[3] E. Shuryak, Phys. Rep. **67**, 71 (1980).
[4] A. Shor, Phys. Lett. B **233**, 231 (1989).
[5] K. Eskola and J. Lindfors, Z. Phys. C **47**, 141 (1990).
[6] M. Asakawa and T. Matsui, Phys. Rev. D **43**, 2871 (1991).
[7] P. Ruuskanen, in *Quark Matter 90*, Proceedings of the Conference, Menton, France, 1990, edited by J. P. Blaizot *et al.* [Nucl. Phys. **A525**, 255c (1991)].
[8] R. Hwa and K. Kajantie, Phys. Rev. D **32**, 1109 (1985).
[9] K. Kajantie *et al.*, Phys. Rev. D **34**, 2746 (1986).
[10] J. Cleymans, K. Redlich, and H. Satz, Z. Phys. C **53**, 517 (1991).
[11] K. Haglin, C. Gale, and V. Emel'yanov, Phys. Rev. D **46**, 4082 (1992).
[12] E. Braaten, R. D. Pisarski, and T. Chiang Yuan, Phys. Rev. Lett. **64**, 2242 (1990).
[13] T. Altherr and P. V. Ruuskanen, Nucl. Phys. **B380**, 377 (1992).
[14] J. Bjorken, Phys. Rev. D **27**, 140 (1983).
[15] K. Geiger, Phys. Rev. D **46**, 4986 (1992).
[16] F. Karsch, Z. Phys. C **38**, 147 (1988).
[17] R. Ruckl, Phys. Lett. **64B**, 39 (1976).
[18] C. Gale and J. Kapusta, Phys. Rev. C **35**, 2107 (1987).
[19] E. Byckling and K. Kajantie, *Particle Kinematics* (Wiley, New York, 1973), p. 23.
[20] C. Gale and J. Kapusta, Phys. Rev. C **40**, 2397 (1989).
[21] K. L. Haglin, Ann. Phys. (N.Y.) **212**, 84 (1991).
[22] J. F. Grivaz *et al.*, Phys. Lett. **61B**, 400 (1976).
[23] H. A. Weldon, Phys. Rev. Lett. **66**, 293 (1991).
[24] J. F. Donoghue, C. Ramirez, and G. Valencia, Phys. Rev. D **39**, 1947 (1989).
[25] H. van Dam and M. Veltman, Nucl. Phys. **B22**, 397 (1970).
[26] V. Srinivasan *et al.*, Phys. Rev. D **12**, 681 (1976).
[27] S. D. Protopopescu *et al.*, Phys. Rev. D **7**, 1279 (1973).
[28] J. Leader and E. Predazzi, *An Introduction to Gauge Theories and the "New Physics"* (Cambridge University Press, Cambridge, England, 1982).
[29] P. Danielewicz and M. Gyulassy, Phys. Rev. D **31**, 53 (1985).
[30] T. DeGrand and D. Toussaint, Phys. Rev. D **25**, 526 (1982).
[31] J. Kapusta, P. Lichard, and D. Seibert, Phys. Rev. D **44**, 2774 (1991).
[32] J. Kapusta, Phys. Lett. **136B**, 201 (1984).
[33] J. Kapusta, Phys. Lett. **118B**, 343 (1982).
[34] E. Braaten and R. D. Pisarski, Phys. Rev. Lett. **64**, 1338 (1990).
[35] L. Heller, in *Proceedings of the Pittsburgh Workshop on Soft Lepton Pair and Photon Production*, Pittsburgh, 1990 (Nova Science, New York, 1992).
[36] S. M. H. Wong, Z. Phys. C **53**, 465 (1992).
[37] J. Gaber and H. Leutwyler, Phys. Lett. B **184**, 83 (1987).
[38] C. Gale and J. Kapusta, Nucl. Phys. **B357**, 65 (1991).
[39] K. Haglin, C. Gale, and V. Emel'yanov (unpublished).
[40] R. P. Feynman, Phys. Rev. **76**, 769 (1949).